Research Square

Preprints are preliminary reports that have not undergone peer review.
They should not be considered conclusive, used to inform clinical practice,
or referenced by the media as validated information.

Highly Transient Thermal Runaway and Gas Emission Dynamics of LiFePO 4 Batteries under Extreme Overcharge Conditions

Yajun Huang
Nanjing Tech University
Zhengbao Wu
Nanjing Tech University
Tiantian Wang
Nanjing Tech University
Zhaozhao Chi
Nanjing Tech University
Junling Wang
Nanjing Tech University
Yu Fan
Nanjing Tech University
Yujie Shi
Nanjing Tech University
Jialong Liu
Nanjing Tech University
Zhirong Wang
wangzhirong@njtech.edu.cn

Nanjing Tech University

Research Article

Keywords: Thermal runaway, Lithium-ion batteries, Overcharge, Gas venting

Posted Date: July 2nd, 2026

DOI: https://doi.org/10.21203/rs.3.rs-10052084/v1

License: This work is licensed under a Creative Commons Attribution 4.0 International License.
Read Full License

Additional Declarations: No competing interests reported.

Highly Transient Thermal Runaway and Gas Emission Dynamics of $LiFePO_4$ Batteries under Extreme Overcharge Conditions

Yajun Huang [a,b], Zhengbao Wu[a], Tiantian Wang [b], Zhaozhao Chi [b], Junling Wang [a,c], Yu Fan [a], Yujie Shi[a], Jialong Liu [a], Zhirong Wang[b*]

[a] *College of Safety Science and Engineering, Nanjing Tech University, Nanjing, Jiangsu 211816, China*

[b] *College of Emergency Management, Nanjing Tech University, Nanjing, Jiangsu 211816, China*

[c] *Department of Architecture and Civil Engineering, City University of Hong Kong, Tat Chee Avenue, Kowloon, Hong Kong, China*

Abstract

The large-scale application of lithium-ion batteries in new energy systems positions their fire safety under extreme environments as a primary focus. Overcharge-induced thermal runaway (TR), particularly under highly transient and irregular electrical conditions, serves as a critical safety bottleneck. This study systematically investigates the TR, pyrolysis, and gas emission dynamics of commercial 15 Ah LFP batteries driven by extreme high-rate overcharging (up to 12C). By employing multi-parameter synchronous monitoring—including temperature, voltage, gas release, infrared thermography, and particularly extreme mechanical impact—the coupled thermo-electrical-mechanical behaviors of battery TR in non-equilibrium states are comprehensively elucidated. The results indicate that as the charging rate increases, the battery is forced into a highly transient state where the TR triggering time significantly shortens and heat accumulation effects intensely accelerate. Notably, under these extreme conditions, more prominent destructive characteristics are manifested. Specifically, a highly rapid maximum surface temperature (Tmax) surge to 453 °C and an accumulated heat of 140 kJ are generated at the 6C rate, while an extreme mechanical structural expansion force reaches 9300 N at 12C. This research uncovers the novel physical and chemical mechanisms governing battery TR under extreme thermo-electric coupled conditions, offering advanced diagnostic insights and a theoretical framework for the fire safety of next-generation energy systems.

Keywords: Thermal runaway; Lithium-ion batteries; Overcharge; Gas venting

*Corresponding author, Email address: wangzhirong@njtech.edu.cn (Z. Wang)

Nomenclature

Abbreviations		T_3	side-surface measured temperature of battery (℃)
TR	thermal runaway	T_{peak}	time to peak rate
DV	digital video	T_x	intermediate temperature of LIBs TR
SEI	solid electrolyte interphase	T_{max}	maximum temperature of the battery surface (℃)
EV	electric vehicle	T_{onset}	starting TR temperature of battery (℃)
LIB	lithium ion battery	T_0	initial temperature (℃)
RUL	remaining useful life	T_b	corresponding voltage V_p (℃)
VMD	variational mode decomposition	Q	total heat production (J)
RVM	relevance vector machine	Q_{rev}	reversible heat (J)
LFP	lithium iron phosphate	Q_{ohm}	joule heat (J)
TOC	total organic carbon	Q_{side}	heat generated by side reactions before TR (J)
CC	constant current	Q_{chem}	heat generated by side reactions during TR (J)
CV	constant voltage	Q_s	heat generated by the short circuit (J)
DMC	anhydrous dimethyl carbonate	Q_p	dissipates heat (J)
SEM	scanning electron microscope	M	battery weight (kg)
FED	fractional effective dose	C_p	battery heat capacity (KJ/ (kg K))
Variables		SOC_{T_0}	SOC of T_0
T_1	front-surface measured temperature of battery (℃)	SOC_{T_b}	SOC of T_b
T_2	back-surface measured temperature of battery (℃)	$SOC_{T_{onset}}$	SOC of T_{onset}

1. Introduction

As global climate change is perceived as a significant threat to human society, carbon neutrality has been elevated to a national strategy by an increasing number of countries, and a commitment is being made to the construction of a carbon-free future [1-4]. Distinct from traditional fossil energy [5], lithium-ion batteries (LIBs) have been established as the core electrochemical energy carriers for replacing fossil fuels in transportation and energy storage sectors, facilitated by their prominent advantages such as high energy density [6], long cycle life [7], and recyclability [8]. To date, more than 90% of electrochemical energy storage has been occupied by LIBs [9]. However, the safety of LIBs is still regarded as a severe challenge that restricts their large-scale application [10, 11]. During storage, transportation, and usage, TR can be triggered by any form of abuse, subsequently leading to serious accidents such as fires and explosions [12-14]. Specifically, under extreme destructive conditions involving thermal [15-18], electrical [19-22], or mechanical [23-26] factors, violent exothermic chemical reactions are easily induced among internal electrode materials and electrolytes. This leads to continuous heat accumulation and the eventual induction of TR accidents [27-29]. This safety hazard not only has hindered the further development and application of LIBs (including lithium-ion capacitors) [30], but also has necessitated an urgent and in-depth investigation into TR characteristics and the proposal of more efficient fire prevention measures for battery energy storage systems [31].

The TR of LIBs involves a multi-stage chain evolution process, including SEI film decomposition, anode-electrolyte reaction, separator melting, cathode decomposition and electrolyte oxidation, binder decomposition, and the burst and termination of TR [32, 33]. Given its severe threat to battery safety, extensive research has been conducted on battery thermal model structures and related experiments to minimize the occurrence of TR. Huang et al. [33] investigated the jetting characteristics of LIBs under different fire source-to-wall distances and found that the battery fire during the combustion process can be divided into three stages: (I) ignition and stable combustion, (II) multiple

intermittent jet fires and stable combustion, and (III) combustion decay and extinction. Inspired by figs, Wang et al. [34] designed carbon microspheres. This unique structure reduced the maximum heating rate of the lithium-ion battery by 54.2% while maintaining high electrochemical performance. Lin et al. [35] systematically summarized the design methods, material preparation, pre-lithiation effects, advantages, and remaining challenges of anode pre-lithiation, cathode pre-lithiation, and the pre-lithiation of other functional components, and analyzed their feasibility. Arshad et al. [36] conducted a life cycle assessment (LCA) to compare four emerging and commercial battery types (lithium-sulfur (Li-S), magnesium-sulfur (Mg-S), sodium-ion (Na-ion), and nickel-metal hydride (NiMH)). The results showed that Mg–S batteries exhibited the lowest environmental impact and the highest robustness across multiple impact categories, whereas NiMH batteries contributed the most to greenhouse gas emissions and nuclear energy demand. To address the issue of low estimation accuracy caused by complex estimation models in current LIB remaining useful life (RUL) prediction, Chen et al. [37] proposed an RUL prediction method based on variational mode decomposition (VMD) and relevance vector machine (RVM), aiming to reduce the safety risks associated with battery failures through high-precision lifespan prediction. Galushkin et al. [38] identified three main exothermic reactions of battery TR: (1) the release reaction of electrochemical energy accumulated during charging and discharging; (2) the lithium reaction on the surface of cathode active material microparticles; and (3) the composite reaction, consisting of the cathode oxygen evolution reaction and the electrolyte oxidation reaction.

Building upon the substantial research achievements in the multi-stage evolution mechanisms, thermal modeling, and experimental characterization of TR in LIBs, significant attention has been devoted to overcharge-related issues [39-41]. This focus is driven by the fact that overcharge is one of the most prevalent electrical abuse modes, and the TR it triggers is characterized by high suddenness and extreme hazard. Previous studies conducted by various scholars regarding the overcharging of different battery configurations—including pouch, prismatic, and cylindrical cells—are summarized in Table 1.

Notably, within the research on overcharge-induced TR of pouch LIBs, the majority of previous studies have focused on batteries with low capacities, and the applied overcharge rates have been generally low. Consequently, research reports regarding the safety performance of relatively high-capacity pouch batteries under high C-rates remain relatively scarce, leading to an incomplete understanding of the safety impact mechanisms in such scenarios [42]. Furthermore, unlike rigid-cased cells, LFP pouch cells exhibit distinct mechanical boundary behaviors (e.g., severe swelling and sudden rupture) during overcharge, drastically altering heat dissipation and gas venting dynamics. Most existing literature relies solely on temperature variations to assess TR severity, failing to capture the dual lethal threats of intense heat release and toxic gas emissions in confined spaces. With the increasing prevalence of high-capacity and high-rate pouch LIBs in energy storage and automotive sectors, the safety hazards associated with high-rate overcharging have emerged as an urgent issue for the industry. Therefore, it is imperative to analyze the synergistic failure processes of electrodes and electrolytes under these specific conditions and to define the critical threshold conditions for TR. Such investigations are expected not only to fill the existing theoretical gaps but also to establish a robust technical foundation for the practical application of high-safety pouch batteries.

Table 1. Summary of previous studies on the overcharge of lithium-ion batteries.

Author	Type	Capacity	Cathode	Contribution
Chen et al. [43]	Prismatic	32Ah	LFP	Passive overcharge early warning method utilizing relaxation swelling force was proposed. Effective warnings were issued 863–884 s before TR through integration with active threshold-based methods.
Mao et al. [44]	Pouch	1.2Ah	MCN532	The degradation mechanisms of electrochemical and thermal stability in $Li(Ni_{0.5}Mn_{0.3}Co_{0.2})O_2$/graphite LIBs after deep overcharging were revealed.
Hu et al. [45]	Pouch	3.9Ah	$LiCoO_2$	A mechanical modeling method for LIBs under limited overcharge abuse was developed to investigate the electrochemical-thermal coupled failure mechanism during the limited overcharge phase.

Ouyang et al. [46]	Prismatic	150Ah 314Ah 150Ah	LFP LFP NMC	The TR characteristics of large-scale energy storage batteries were investigated by referencing overcharge scenarios under thermal and mechanical abuse conditions.
Kong et al. [47]	Cylindrical	3Ah 4.2Ah	LFP Li_2CO_2	A modeling framework was proposed to capture the transition process of LIBs from slight overcharge cycling to TR through the coupling of electrochemical and thermal models.
Yan et al. [48]	Cylindrical	2Ah 2.5Ah 3Ah	NCM NCM NCM	Eight types of commercial 18650 ternary (NCM) lithium-ion batteries were selected, and their TR risks were systematically evaluated under both low-current (10 V-3 A) and high-current (10 V-6 A) overcharge conditions.

To bridge these critical gaps, the TR characteristics of 15 Ah pouch LFPs under various charging rates (1C, 2C, 6C, and 12C) are investigated in this work. The evolution of voltage, temperature, swelling force, gas components, and heat accumulation during the overcharging process are analyzed in detail, through which the impact of C-rates on battery safety risks is clearly elucidated. The findings of this research provide a significant reference for subsequent fire safety design and emergency response strategies for energy storage systems.

2. Experimental section

2.1 Battery parameters

To ensure practical engineering reference value, commercial 15 Ah LFP power batteries were selected as the research object. By virtue of their excellent thermal stability and cost advantages, this specification of LFP batteries has been widely applied in mass-produced models by several leading new energy vehicle manufacturers, including BYD. It is mainly composed of aluminum laminated films, anode and cathode materials, separators, electrolytes, additives, and other components [49]. Detailed parameters are shown in Table 2. To ensure battery stability, the batteries were cycled three times using a Neware battery tester prior to testing, and constant current-constant voltage (CC-CV) charging alongside CC discharging were adopted. Under the CC mode, the batteries were discharged to 2 V at a rate of 0.4 C, followed by charging to 3.65 V at the same rate. Subsequently, CV mode was applied for charging until the current decreased to 0.05 C.

Table 2. Parameter information of the pouch LFP battery.

Specification	Value
Cathode	Lithium Iron Phosphate ($LiFePO_4$)
Anode	Graphite
Capacity	15Ah
Dimensions (length × width × height)	80 mm*15 mm*145 mm
Nominal voltage	3.2 V
Mass	about310 g
Discharge cut-off voltage	2 V

2.2 Apparatus and methods

The schematic diagram of the experimental apparatus is shown in Fig. 1(a-c). The entire experiment was conducted in an experimental chamber with dimensions of 2.2 m × 2.2 m × 2 m. Devices including the battery, pressure sensor, and mica plates were installed on three metal plates. Mica plates, possessing excellent heat resistance and low thermal conductivity, are key components for enhancing the safety redundancy of battery systems [50, 51]. The metal plates were secured by nuts and screws. The battery and mica plates were placed vertically between two metal plates, while the pressure sensor was positioned between the second and third metal plates in the same orientation. Thermal insulation tools were installed on both sides to prevent excessive heat dissipation from the metal plates. Subsequently, four locking nuts were utilized to fix the battery, ensuring tight contact between the mica plates and the battery, while simultaneously preventing the thermocouples from detaching due to battery swelling. K-type thermocouples were used to measure the battery surface temperature. The temperature range of the thermocouples is 0–1100 ℃ with an accuracy of ± 1.5 ℃, and the sampling rate of the data logger is 1 Hz, which ensures the accurate capture of thermocouple signals, vital for monitoring temperature changes. To capture the TR process, a Sony FDR-AX45A camera and a Telops Fast M200 infrared thermal imager were employed to capture digital photos and infrared thermal images, respectively. A 9100FIR portable Fourier transform infrared gas analyzer was utilized to detect and analyze the smoke components around the experimental chamber. All equipment was started at the beginning of the experiment to ensure the temporal synchronization of data collection and experimental observation.

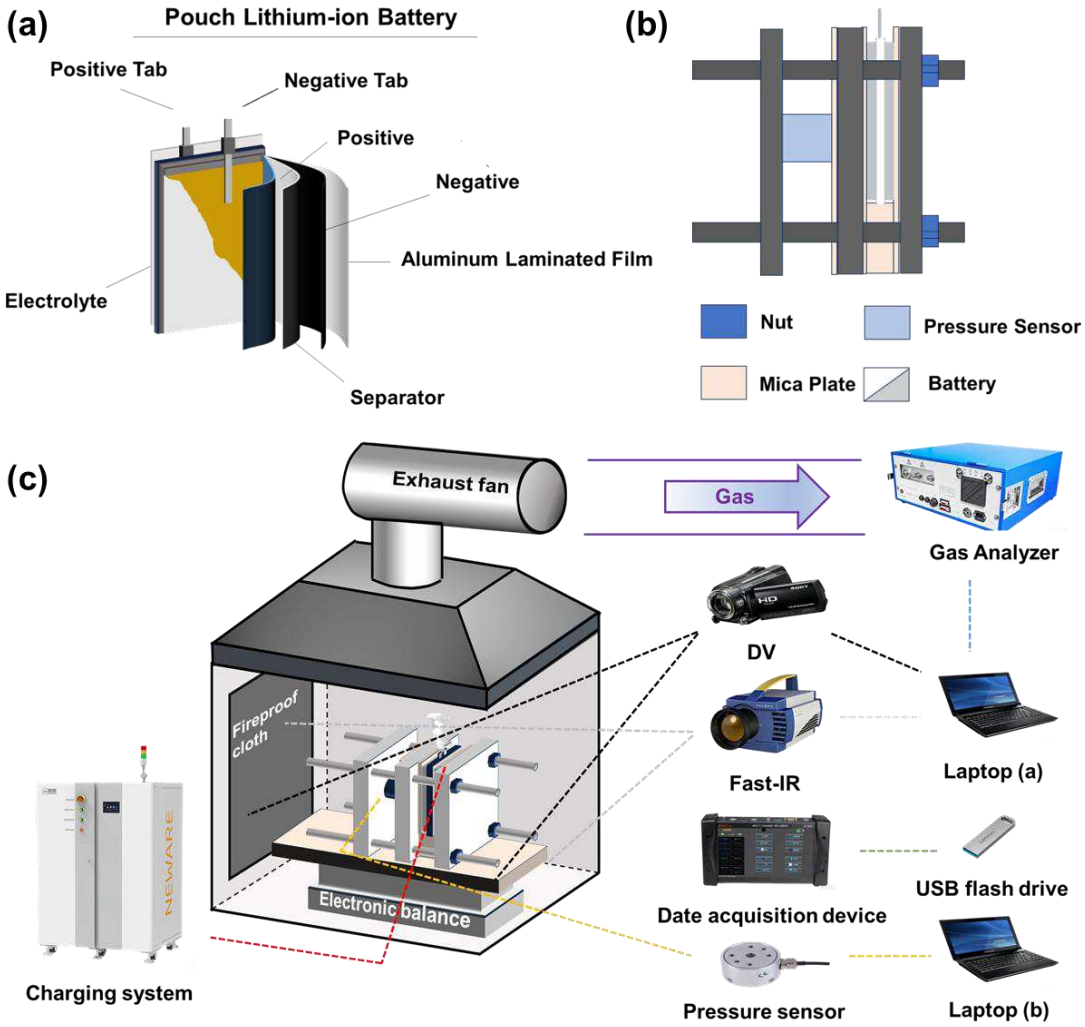


Fig. 1. Schematic of the experimental system: (a) Battery structure, (b) Sensor locations, (c) Overall platform.

2.3 Electrode characterization

Upon completion of the overcharge tests, all batteries from the five experimental groups were allowed to cool to ambient temperature. To prevent any side reactions with moisture or oxygen, the cells were transferred into a high-purity argon-filled glove box (H_2O < 0.1 ppm, O_2 < 0.1 ppm) for safe disassembly. The positive active material (adhered to the aluminum foil) were carefully extracted and subsequently immersed in anhydrous dimethyl carbonate (DMC), followed by multiple rinses to thoroughly remove residual electrolyte salts and decomposition products. After being vacuum-dried, the samples were tailored and prepared for scanning electron microscopy (SEM) to evaluate the morphological degradation and structural evolution under different overcharge rates.

3. Results and discussion

3.1 Material characteristics

To deeply elucidate the microscopic failure mechanisms induced by various overcharge rates, the morphological evolution of the cathode is systematically investigated utilizing SEM and EDS. As illustrated in Fig. (a), in the pristine state, relatively regular secondary spherical structures are exhibited by the particles, which are characterized by dense surfaces and clear boundaries. Close contact between particles is maintained, and no obvious fragmentation or agglomeration is observed. As shown in Fig. (b-c), when the rate is increased to 1C and 2C, slight surface roughening on the particles begins to be observed. The boundaries of the spherical particles are gradually blurred, and the dissociation of some secondary particles is manifested. However, as depicted in Fig. (d), a critical morphological transition is observed at the high overcharge rate of 6C. Intense localized overheating is indicated by drastic changes, including severe particle agglomeration, surface fusion, and the disappearance of primary particle boundaries. This is primarily attributed to the massive Joule heat and the accelerated exothermic side reactions at the electrode-electrolyte interface, which are triggered by rapid high-voltage polarization. Microscopic localized TR is induced by the accumulated thermal energy, by which the binder is melted and active particles are fused; thus, ionic transport channels are significantly blocked. As presented in Fig. (e), under the highest rate of 12C, the most severe degree of structural destruction is reached. The original morphology of the particles is almost completely lost, and a complex structure characterized by the coexistence of severe fragmentation and agglomeration is exhibited. The surfaces of larger particles are covered by massive fine debris, and an obvious secondary accumulation is formed. The progressive damage of the electrode materials during high-rate charge-discharge processes is underscored by these morphological changes, through which the conductivity is decreased and the degradation of the active materials is accelerated. Ultimately, the stability of the battery is compromised.

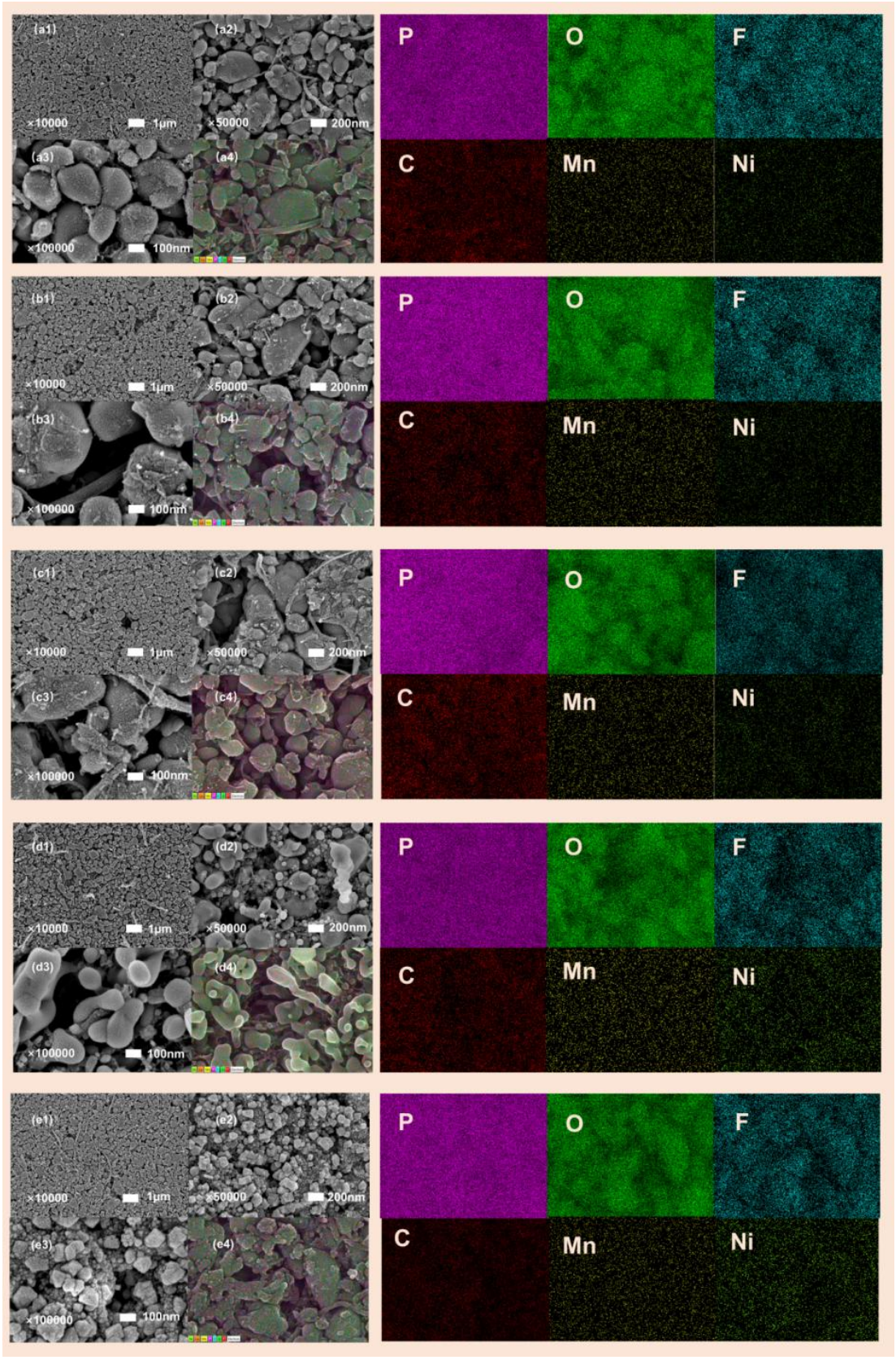


Fig 2. SEM images of the surface morphology and microstructure of the positive electrode under various conditions: (a) fresh; (b) 1C; (c) 2C; (d) 6C; (e) 12C.

The content distribution characteristics of internal C, O, F, P, Mn, and Ni under different conditions are revealed in Fig. 3. Combined with the previous microscopic morphology and elemental mapping results, it can be further clarified that: under the coupled effect of battery overcharge and charging rate, the main elemental composition of the electrode has not undergone a fundamental chemical transformation. The previously observed degradations, such as particle fragmentation and interfacial by-product deposition, are classified merely as local structural changes, and the overall elemental mass fraction characteristics of the electrode remain unaltered.

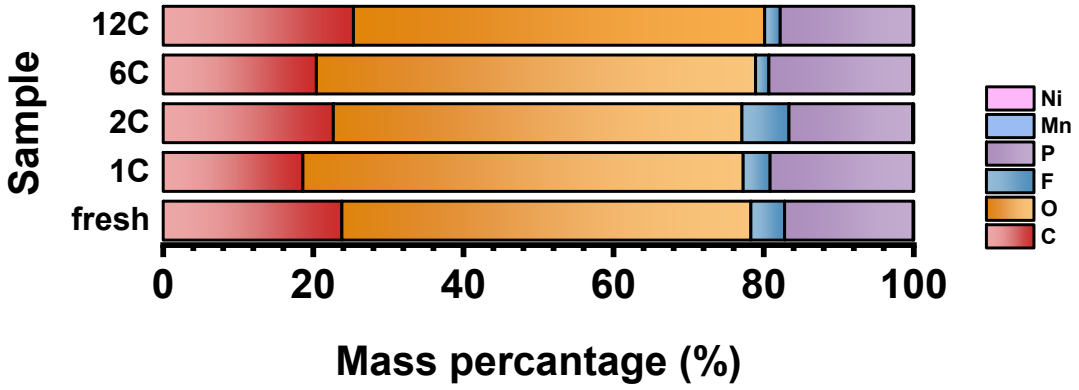


Fig 3. Elemental composition of 15 Ah batteries at various charging rates.

3.2 TR characteristics during overcharge

3.2.1. Temperature and voltage variations in TR

The evolution of surface temperature and internal voltage of the 15 Ah battery under overcharge at different rates is compared in Fig. 4. With the side containing the positive tab of the LIB designated as the front, T1 is recorded as the surface temperature measured on the front of the LIB, T2 as the surface temperature on the back, and T3 as the surface temperature on the positive tab side. Generally, the following three stages are experienced by the LIB during overcharging:

Stage I: The normal charging process is maintained before the voltage reaches inflection point A. At this time, the surface temperature gradually increases with time, the temperature curves are basically consistent, and the temperatures measured at the three locations are also identical. Subsequently, the voltage gradually decreases after passing inflection point A and eventually reaches inflection point B.

Stage II: A sharp increase in voltage is observed after passing inflection point B, ultimately reaching inflection point C (maximum voltage). The voltage increase is

attributed to the partial shrinkage and collapse of the separator caused by continuous overcharging. The rise in battery temperature is aggravated by this process.

Stage III: A sharp drop in voltage is exhibited after inflection point D, followed by a slow decline, eventually reaching 0 V. This stage is accompanied by the extensive shrinkage and collapse of the battery separator, leading to a large-scale internal short circuit. Once an internal short circuit occurs, the battery is rapidly heated by the Joule heat generated from the high current, thereby inducing additional exothermic reactions and further elevating the battery temperature. The battery temperature then slowly decreases after reaching its peak.

TR is triggered in all four batteries shown in the figure. It is easily observed that under 1C overcharge, the LIB voltage initially remains stable, slowly rises to 25.5 V, and then drops, with the process consuming a longer time. As the rate is elevated (2C, 6C, 12C), the voltage stabilization stage is gradually shortened, and the temperature rise rate is drastically accelerated. The peak temperature at 2C overcharge reaches 324.2 ℃, while at 6C and 12C, it rapidly surges above 400 ℃. Furthermore, the time required to reach the peak temperature has been shortened from approximately 1300 s at 1C to roughly 600 s, 170 s, and 150 s (corresponding to 2C, 6C, and 12C, respectively). The fundamental cause of TR induced by overcharging is identified as lithium deposition on the anode, meaning that the migration rate of lithium ions exceeds the intercalation capacity of the anode during high-rate charging, forcing them to be reduced to metallic lithium on the surface. Severe reactions between this layer of highly active deposited lithium and the electrolyte are triggered, by which the SEI film is destroyed and a large amount of heat and flammable gas are released; meanwhile, the separator is prone to be pierced by the continuous growth of lithium dendrites, inducing micro-short circuits. As heat and gas continuously accumulate, TR accidents are ultimately induced. When charging at 1C and 2C rates, lithium dendrites are generally not formed, and uniform lithium films are primarily observed. Conversely, under ultra-high rate charging (6C, 12C), a large number of slender and sharp lithium dendrites are generated, by which the separator is easily pierced, triggering internal short circuits [52].

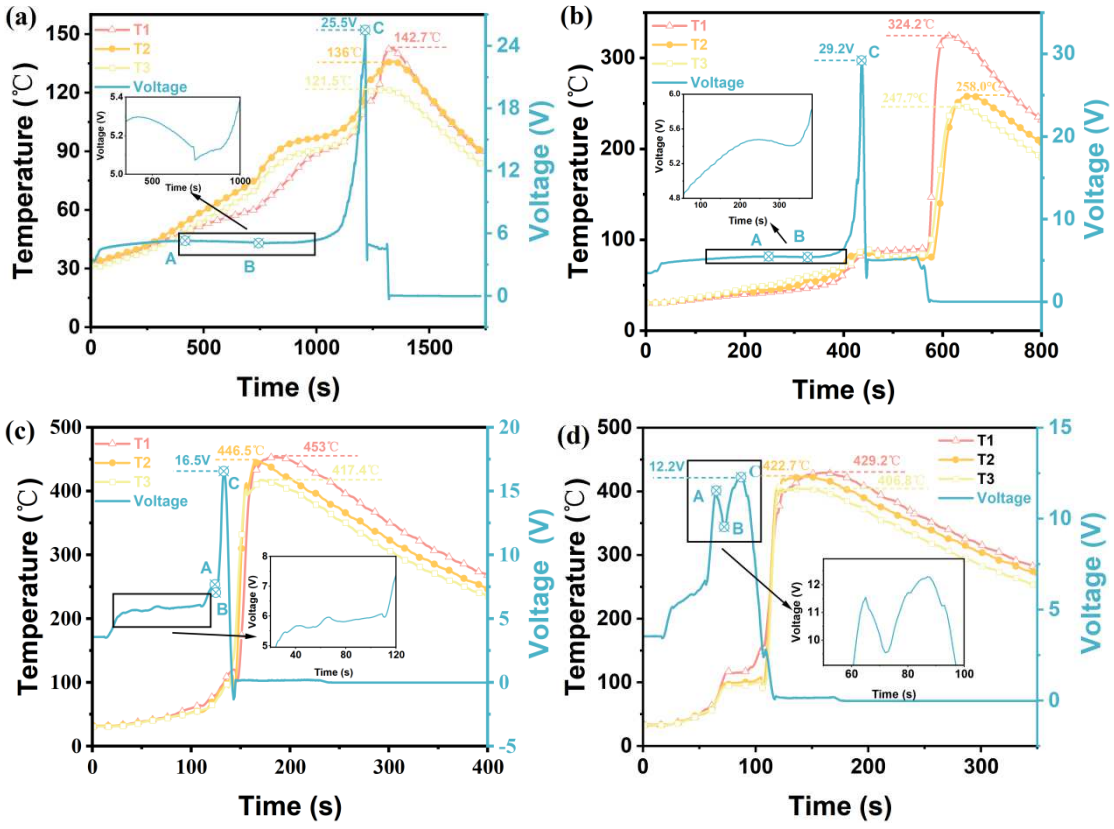


Fig 4. Evolution of surface temperature and internal pressure of 15 Ah batteries at various charging rates: (a) 1C; (b) 2C; (c) 6C; (d) 12C.

3.2.2. Evolution of TR During Overcharge

The TR process of the 15 Ah battery under different charging rates is illustrated in Fig. 5. As shown, sporadic sparks are observed at 1208 s for the battery at the 1C rate, followed by a small amount of smoke until the smoke disappears. No significant TR is observed at this rate. In contrast, cells at 2C, 6C, and 12C exhibited abrupt, heavy white smoke emissions at 565 s, 135 s, and 100 s, respectively, with the venting intensity escalating at higher charging rates. At this moment, it is observed that the smoke injection angle near the battery side is horizontal, while the smoke further away is elevated by buoyancy. Within the subsequent 5–10 s, smoke is stably vented by the battery, after which it gradually diminishes.

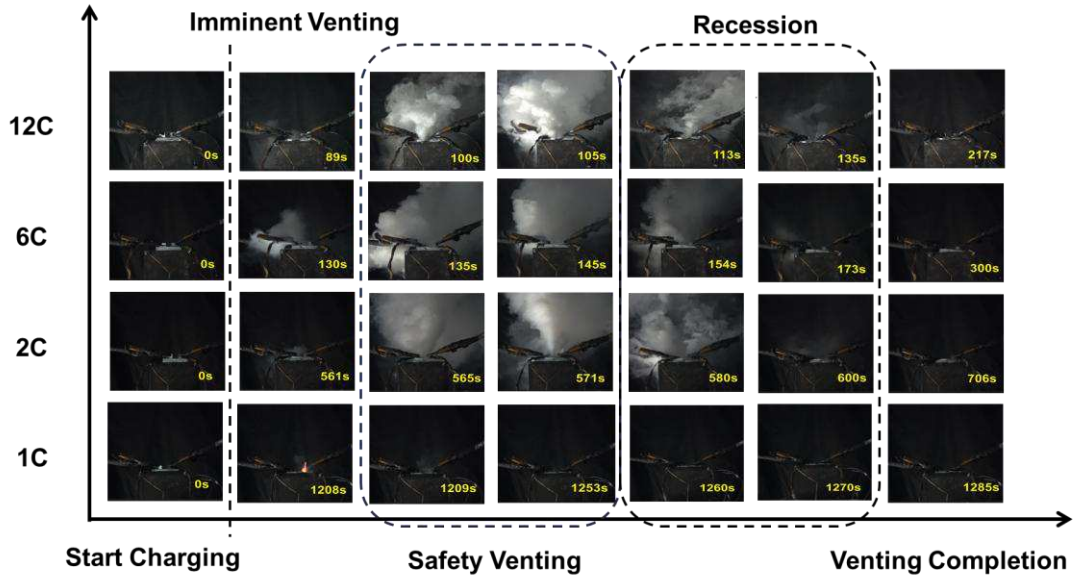


Fig 5. TR images of 15 Ah batteries at various discharge rates.

The temperature field evolution trend of TR propagation in 15 Ah LFPs under different charging rates are intuitively presented through infrared thermal imaging in Fig. 6. Combined with the temperature thresholds of internal side reactions and thermodynamic equilibrium, the regulatory mechanism of charging rate on the TR process can be elucidated: when the battery is overcharged at the 1C rate, the temperature field is shown by thermal imaging to gradually evolve from the initial state at 996 s, reaching a peak of 106.5 ℃ at 1143 s. This temperature range corresponds to the decomposition of the SEI film and the initial side reactions between the anode and electrolyte, but the decomposition temperature threshold of the LFP cathode material has not been reached. During this stage, the heat generation rate of 1C charging is relatively low, and the heat diffusion rate is maintained higher than the internal heat accumulation rate due to the large heat dissipation area of the aluminum laminated film. Therefore, the temperature drops in the later stage, and the battery is merely suspended in the preheating trigger stage of TR, without initiating the violent exothermic reactions involving the cathode.

At the 2C rate, the time nodes of thermal imaging are significantly compressed: the battery remains in the preheating state at 555 s, but the temperature surges to 289.8 ℃ after merely 10 s. This abrupt change corresponds to the fact that the electrode

polarization is aggravated by the large 2C current. The rupture of the SEI film and the heat accumulation from anode side reactions are accelerated by the elevated local overpotential, which enables the temperature to rapidly exceed the decomposition temperature of the LFP cathode, thereby triggering the phase transition and oxygen release reaction of $LiFePO_4$. Violent oxidation reactions are induced between the released active oxygen and the electrolyte, indicating that the violent TR stage has been entered.

The acceleration effect of rate on the process is further manifested by thermal imaging at high rates (6C, 12C): at 6C charging, the temperature for complete SEI decomposition is reached in merely 126 s, and the cathode decomposition stage is entered at 137 s as the temperature breaks through 206.2 ℃. Under 12C charging, this is even further compressed, with preheating initiated at 83 s and 224.2 ℃ reached at 104 s. This is explained by the exponential increase in current density at high rates, where Joule heat increases alongside the current. Simultaneously, uneven lithium-ion distribution is caused by concentration polarization, and micro-short circuits are triggered by lithium dendrite growth on the anode surface. The time window for breaking through the temperature threshold is further shortened by this additional heat generation. Furthermore, the concentrated distribution of local high-temperature zones in the thermal images reflects the unevenness of the temperature field at high rates, where local hotspots preferentially trigger side reactions, further intensifying the TR propagation efficiency.

In summary, high C-rates not only intensify heat generation but also compress the temporal intervals between TR stages. This bolsters the positive feedback loop between thermal accumulation and side reactions, ultimately accelerating the transition from initial triggering to catastrophic TR.

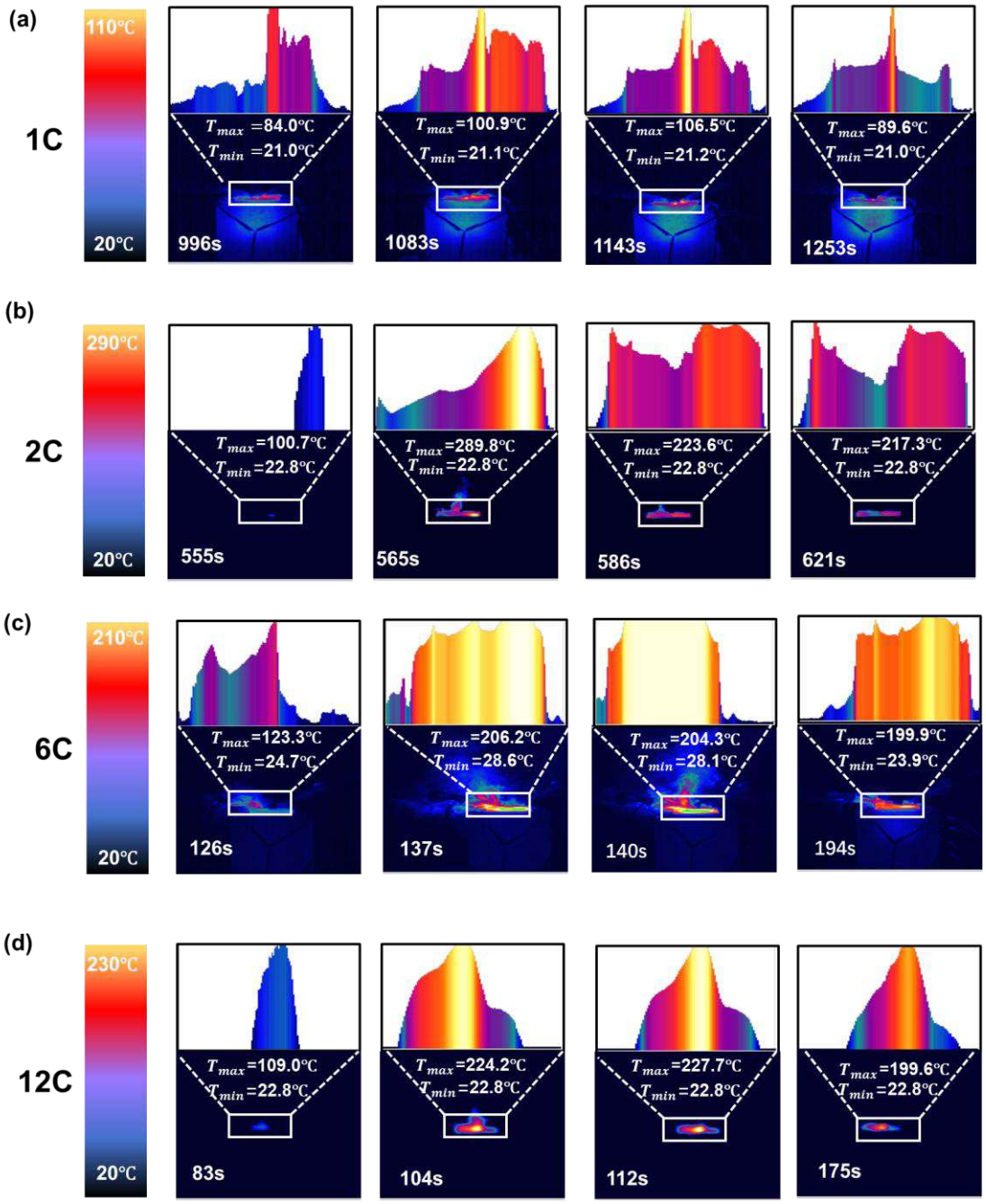


Fig 6. Comparison of infrared thermography during the TR process at various C-rates: (a) 1C; (b) 2C; (c) 6C; (d) 12C.

3.2.3. Dynamic response of overcharge swelling force under rate dependence

The mechanical evolution of the LIB module from overcharge to TR under different charging rates is displayed in Fig. 7. To secure the battery pack and ensure consistent initial experimental conditions, the initial swelling force of the module has been set to 150 N via screw adjustment prior to the experiment. As shown in Fig. 7, the system structure remains relatively stable in the early stage of the experiment, with the

system swelling force fundamentally stabilized at the initial level. As the rate increases, the onset time of severe swelling is drastically shortened, plunging from 740 s at 1C to 66 s at 12C. The most notable change is that a monotonic upward trend is exhibited by the peak swelling force as the charging rate increases, reaching 6791 N, 7016 N, 7781 N, and 9300 N, respectively. A strong dependence of overcharge swelling behavior on charging rate is clearly indicated by this phenomenon, confirming that the severity and instability of the mechanical response are significantly exacerbated by high rates.

Further analysis of the force change rate reveals that the absolute values of the force change rate during both the rising and falling stages are synchronously and substantially increased as the charging rate rises. The peak rate during the rising stage surges from 15 N/s at 1C to 940 N/s at 12C. This sharp ascent is jointly driven by the rapid expansion of the anode graphite lattice caused by fast lithium intercalation and the explosive gas generation from the electrolyte accelerated by rapid heat accumulation. The continuous chain effects of electrolyte decomposition are made more pronounced by the rapid heat accumulation induced by fast overcharging, leading to a sudden surge in swelling force due to short-term gas buildup. Moreover, the risk to the overall structure is augmented by the structural strain resulting from excessive delithiation at high rates. Severe force change rate fluctuations near the peak, especially at 6C and 12C, uncover a stronger blasting nature, signifying that more severe structural and mechanical failure risks are induced by high-rate overcharging.

In conclusion, the strong sensitivity of the swelling force and its change rate to the charging rate demonstrates that while chemical reactions are accelerated by high-rate charging, the mechanical structural risks of the battery are simultaneously magnified exponentially. More importantly, the abnormal appearance time of the swelling force signal has been proven to be significantly earlier than subsequent fatal TR events such as safety valve venting and internal short circuits. Therefore, direct, sensitive, and early fault warning signals can be provided by online monitoring based on real-time swelling force and its change rate, which holds vital guiding value for constructing dynamic battery mechanical safety monitoring systems [43].

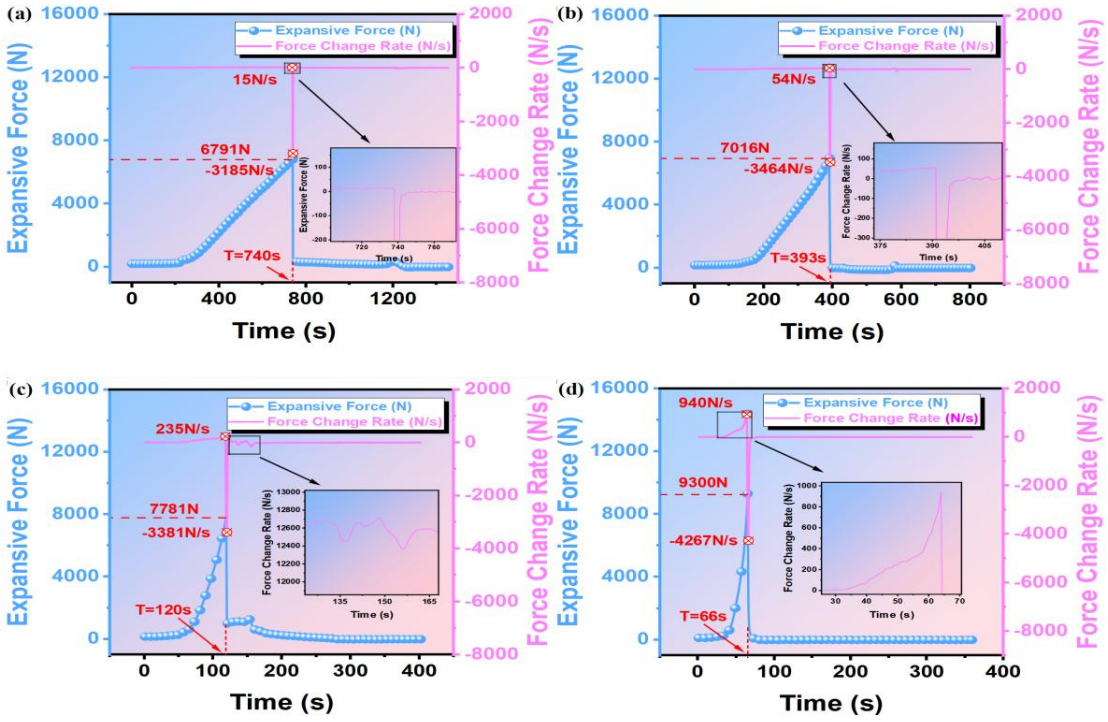


Fig 7. Mechanical evolution during the TR propagation process at various C-rates: (a) 1C; (b) 2C; (c) 6C; (d) 12C.

3.2.4. Gas analysis in TR

Flames are generally not produced during the TR process of LFP batteries; instead, a massive amount of smoke is released [12]. Therefore, revealing the real-time smoke composition and concentration is crucial. For instance, HF is produced by the decomposition of lithium salts in the electrolyte at high temperatures; CO is generated by the incomplete combustion of the organic electrolyte with electrode materials under hypoxic conditions; SO_2 is yielded by the high-temperature decomposition of sulfur-containing additives or impurities; and hydrocarbon gases (CH_4, C_2H_4, C_3H_6, etc.) are formed through the pyrolysis and polymerization of electrolyte solvents. In this study, C_2H_4, TOC, CO, and CO_2 are selected as detection targets, and their concentration change data during the experiment are plotted Fig. 8. It can be seen that the peak appears at around 1000 s at the 1C rate; at 2C, the peak emerges around 500 s; at 6C, the peaks are concentrated around 200 s; and at 12C, they are clustered around 100 s. That is, the higher the overcharge rate, the shorter the TR trigger time. It is indicated that the TR process of the battery is significantly accelerated by high-rate overcharging, causing exothermic processes such as electrolyte decomposition and electrode reactions to

occur earlier and more collectively. It should be noted that a time "delay" exists between the data collected by the gas analyzer and the real-time data captured by the DV, which is attributed to the time required for the smoke generated after TR to reach the gas analyzer through the collection device. Observing C_2H_4, the generation amount is highest at the medium rate (2C) and decreases significantly at the high rate (12C). C_2H_4 primarily originates from the pyrolysis and polymerization of carbonate solvents in the electrolyte, and its concentration is reduced due to the competition of reaction pathways at high rates. The TOC concentration initially surges and then slightly drops with the rising rate, reaching a peak around 6C. TOC reflects the decomposition degree of the organic components in the electrolyte, indicating more intense electrolyte cracking at medium and high rates; at 12C, the concentration inversely decreases because the organic component decomposition stage is compressed due to the overly abrupt reactions. CO shares a consistent trend with TOC, with its concentration rising first and then falling as the rate increases, dropping significantly at the high rate (12C). CO is primarily derived from the incomplete combustion of organic components or CO_2 reduction reactions, and its concentration variation is directly correlated with the severity of electrolyte decomposition. The generation of CO_2 remains relatively stable, with peak values stabilizing in the range of 0.06% to 0.062%. This indicates that it primarily stems from early SEI film decomposition or mild electrolyte oxidation, and the overall generation level of CO_2 is not significantly altered by the competition from other reactions (such as CO generation and C_2H_4 cracking) at high rates.

In summary, a positive correlation is established between the LIB overcharge rate and the TR trigger speed. The peak concentrations of organic electrolyte decomposition products (TOC, CO, CH_4) initially increase and then slightly recede with the elevation of the overcharge rate, which not only demonstrates that electrolyte decomposition is exacerbated by high-rate overcharging but also reflects a more abrupt reaction process under extreme high rates. The release proportion of CO_2 is maintained stable across different overcharge rates, acting as one of the characteristic foundational gases for TR in this system.

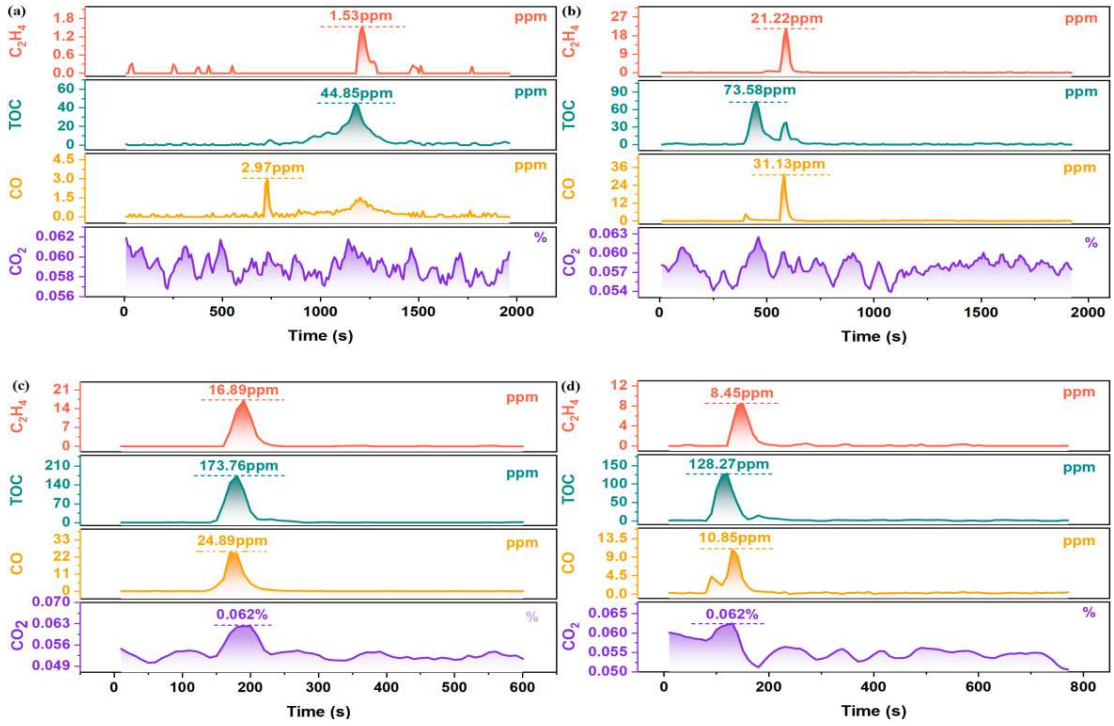


Fig 8. Gas composition characteristics during battery TR at various C-rates: (a) 1C; (b) 2C; (c) 6C; (d) 12C.

3.3 Heat transfer analysis

The preceding analysis of multi-dimensional characteristic parameters during overcharging has demonstrated that the deterioration rate of macroscopic battery performance is significantly aggravated by the increase in charging rate. However, the essence of this failure phenomenon lies in the disruption of the dynamic equilibrium between internal heat generation and external dissipation. To further unveil the fundamental driving force of TR occurrence under different overcharge rates, the perspective is shifted from phenomenological observation to quantitative thermodynamic analysis in this section, and the transient heat transfer mechanisms and heat accumulation laws during battery overcharging are emphatically explored. The heat accumulation at different rates can be calculated according to Eq. (1)–(5) [53]. In the formulas, the total heat generation during overcharge is composed of Q_{rev}、Q_{ohm}、Q_{side}、Q_{chem}、$Q_s$and Q_p. Q_{rev} represents the reversible heat generated by the enthalpy change of electrochemical reactions; Q_{ohm} denotes the Joule heat produced by battery impedance; Q_{side} is the heat generated by internal side reactions prior to TR; Q_{chem} is

the heat generated by internal side reactions during TR; Q_s stands for the heat generated when the battery short-circuits; and Q_p is the heat dissipated by the battery. Considering that the battery is wrapped in thick insulation cotton, it can be approximated to be in an adiabatic state; thus, Q_p can be ignored. The heat calculation methods for each part are shown in the following equations:

$$Q=Q_{rev}+Q_{ohm}+Q_{chem}+Q_s+Q_p \tag{1}$$

$$Q_{rev}+Q_{ohm}=M\cdot C_p\frac{T_b-T_0}{SOC_{T_b}-SOC_{T_0}}\left(SOC_{T_{onset}}-SOC_{T_0}\right) \tag{2}$$

$$Q_{side}=M\cdot C_p(T_{onset}-T_x) \tag{3}$$

$$T_x=T_0+\frac{T_b-T_0}{SOC_{T_b}-SOC_{T_0}}\left(SOC_{T_{onset}}-SOC_{T_0}\right) \tag{4}$$

$$Q_{chem}+Q_s=M\cdot C_p(T_{max}-T_{onset}) \tag{5}$$

In the equations, M is the battery weight; C_P represents the battery heat capacity; the specific heat capacity of the batteries used in this study is taken as 1.1 KJ/(kg·K). Since the temperatures at three locations on the battery are measured for each experimental group, the average value is uniformly adopted for temperature calculations. Here, SOC_{T_0}= 100%, b is an arbitrary point, and T_0 is room temperature, taken as 21 ℃.

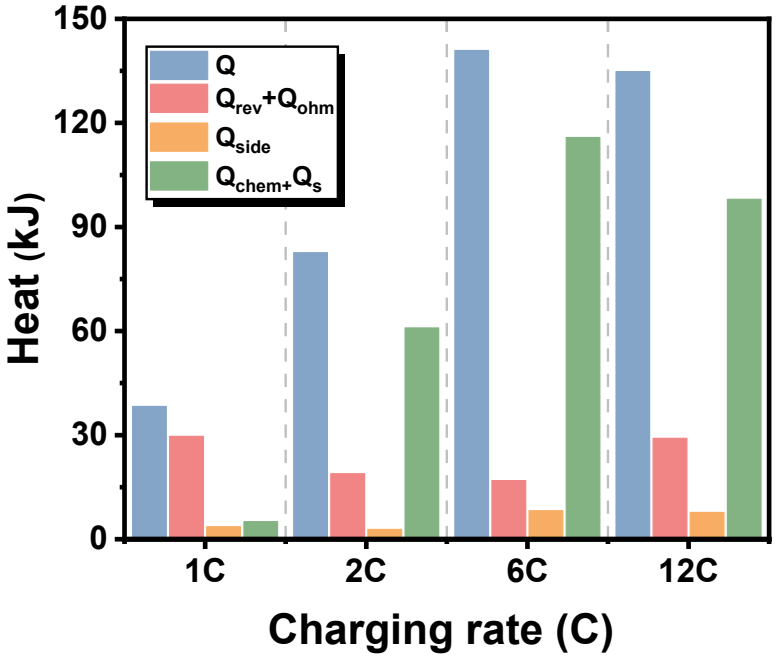


Fig 9. Summary of Q, $Q_{rev}+Q_{ohm}$, Q_{side}, and $Q_{chem}+Q_s$ for batteries during overcharge tests at various rates.

The summary results of heat accumulation for LFP batteries during the overcharge process at 1C, 2C, 6C, and 12C rates are presented in Fig. 9. It is shown by the results that a rapid growth trend is exhibited by the total heat Q with the elevation of the charging rate. Although the total heat drops to 135 kJ at the 12C rate, its value remains more than 3.5 times that of the 1C rate. The underlying reason is that 12C belongs to an ultra-high charging rate, where the charging current is drastically amplified, and the TR trigger rate is extremely fast. The swifter the TR occurs, the shorter the duration of chemical side reactions becomes, resulting in a total accumulation of $Q_{chem}+Q_s$ slightly lower than that at the 6C rate. However, the heat release rate per unit time is significantly elevated, causing the actual TR risk to become even more severe. The sum of reversible heat and Joule heat $Q_{rev}+Q_{ohm}$ presents a certain fluctuation characteristic: at the low 1C rate, the charging duration is longer, and the accumulation of reversible and Joule heat is higher; conversely, at medium-high rates of 2C and 6C, the charging duration is shortened, and the accumulation of this portion of heat is correspondingly reduced. The intermediate temperature T_x prior to TR is maintained at a higher level at 1C and 12C rates, corresponding to higher accumulations of reversible and Joule heat at these two rates; meanwhile, T_x is relatively low at 2C and 6C rates, which is also consistent with the trend of decreased reversible and Joule heat accumulation within this rate interval. This indicates that Joule heat is one of the crucial factors leading to the battery temperature rise before TR. Hence, the heat accumulation of the battery is further intensified by the rebound effect of Joule heat under ultra-high charging rates. The proportion of transitional heat Q_{side} in the total heat is consistently maintained below 10%. As heat generated during the TR transition stage, its impact on the overall trend of heat accumulation is relatively limited. The chemical side reaction heat $Q_{chem}+Q_s$ is identified as the core heat source triggering battery TR: at the 1C rate, this portion of heat is merely 5 kJ, accounting for 13% of the total heat; it surges to 60.8 kJ at the 2C rate; and it exceeds 90 kJ at the 6C and 12C rates. This demonstrates that internal chemical side reactions of the battery are significantly intensified by high charging rates, making the released chemical heat the dominant source of heat for TR,

which is also the core reason why the battery is more prone to severe TR under high-rate charging.

In conclusion, the significant differences are observed in the TR characteristics of LFP batteries overcharged at different rates: at a low rate (1C), the TR process is relatively mild, and the heat released by chemical side reactions is minimal; at medium-high rates (2C and 6C), the severity of TR is significantly aggravated, and the chemical side reaction heat becomes the dominant heat source for TR; at an ultra-high rate (12C), although the total heat slightly decreases due to the shortened reaction time, the heat release per unit time is more concentrated, leading to a significantly elevated battery TR risk.

3.4 Gas toxicity study during TR

The smoke toxicity under different rates is generally evaluated using the fractional effective dose (FED) defined in the international standard (ISO 13571), indicating that its toxic impact is associated not only with gas concentration but also with exposure time. CO and HCN are identified by the FED model as the primary asphyxiant gases, causing cellular hypoxia and subsequently interfering with vital physiological functions. Concurrently, respiratory activity is stimulated by inhaled CO_2, accelerating respiratory depth and frequency, which in turn increases the absorption rate of other toxic substances [54]. The detailed calculation formulas are displayed in Eq. (6-7). Based on the time-varying concentrations of CO, CO_2, and HCN, a smoke toxicity diagram under different rates has been plotted combined with the formulas Fig. 10.

$$X_{FED}=\sum_{t_1}^{t_2}\frac{\emptyset_{CO_2}V_{CO}}{35000}\Delta t_i+\sum_{t_1}^{t_2}\frac{\left(\emptyset_{CO_2}V_{HCN}\right)^{2.36}}{1.2\times10^{6}}\Delta t_i \quad (6)$$

$$\emptyset_{CO_2}=\exp\left(\frac{V_{co_2}}{5}\right) \quad (7)$$

where $\emptyset$ represents the concentration of each gas (μL/L), V stands for the volume fraction of each gas (%), and Δt_i is the time increment (min).

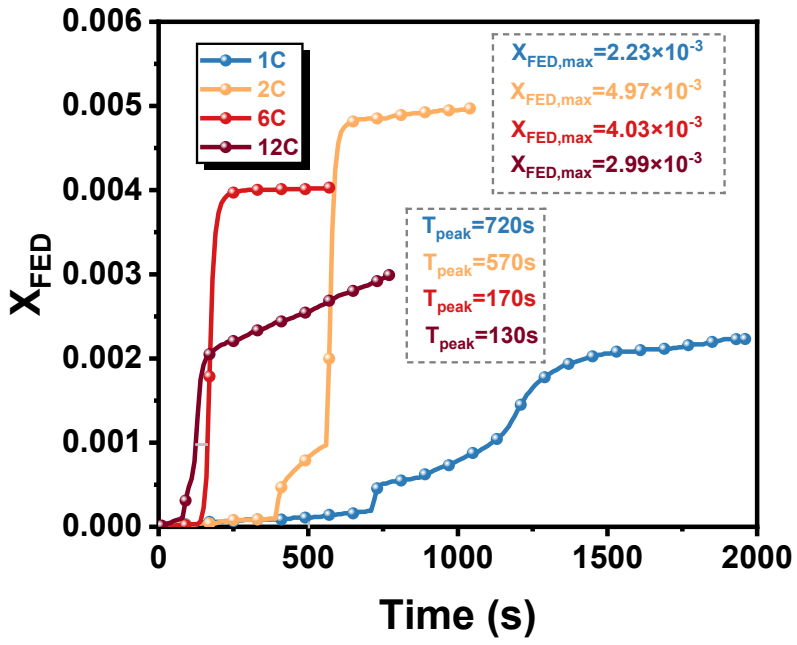


Fig 10. Toxicity of smoke emissions during overcharge tests at various rates.

Overall, no obvious combustion phenomenon has occurred in the four groups of experiments, leading to the released toxic substances being predominantly low-concentration irritant gases; therefore, the corresponding toxicity index is extremely low, and the harm to the human body is deemed negligible. The maximum values of X_{FED} at 1C, 2C, 6C, and 12C rates are recorded as 0.00022, 0.0005, 0.0004, and 0.0003, respectively. When charging at extremely high rates (6C, 12C), the migration of lithium ions is extremely rapid, and side reactions such as anode lithium dendrite formation and electrolyte decomposition are collectively triggered within a short period. However, once part of the reaction materials (e.g., local electrolyte) is rapidly depleted, the rate of subsequent side reactions slows down, making the growth of X_{FED} flatter. Conversely, when charging at the 2C rate, side reactions are continuously accumulated without reaching the point of material depletion saturation; hence, its final X_{FED} ultimately surpasses the values corresponding to 6C and 12C in the later stages.

4. Conclusion

The evolution characteristics of 15 Ah LFP batteries during TR induced by overcharge at different rates (1C, 2C, 6C, 12C) have been systematically investigated in this study through multi-parameter synchronous monitoring methods. From the

perspective of multi-physical field coupling (electrical-thermal-mechanical-gas), the regulatory effects of charging rate on the TR trigger mechanism and disaster intensity have been deeply explored. The main conclusions are summarized as follows:

(1) The core value of mechanical swelling signals in the safety early warning of large-capacity batteries has been clarified. It is discovered by the experiment that the mechanical strain response triggered by overcharge is significantly superior to traditional temperature and voltage signals. Especially at the extremely high 12C rate, the battery swelling force surges to 9300 N prior to the occurrence of TR. The fact that this mechanical inflection point precedes the sudden change in temperature rise slope and the voltage failure inflection point proves that integrating stress sensors into the Battery Management System (BMS) possesses significant engineering importance for achieving early warnings of high-rate overcharging.

(2) The multi-stage evolution law of electrode microscopic morphology degradation has been elucidated. Confirmed by combined SEM and EDS analyses, the mechanical integrity of the electrode is directly determined by the overcharge rate through the regulation of lithium deposition kinetics. With the elevation of the rate, the cathode active particles evolve from marginal microcracks to global pulverization and pore collapse. This structural dissociation at the microscopic level not only blocks the effective migration of ions but is also pinpointed as the physical essence inducing large-scale internal short circuits and driving the transition of TR from local reactions to global chain collapses.

(3) The nonlinear coupling mechanism between heat release characteristics and charging rate has been revealed. Research indicates that the total heat Q released during battery overcharging does not grow linearly with the rate but presents a peak trend at the 6C rate (peak value of 140.9 kJ). Although the total heat generation is slightly reduced under 12C conditions, the heat release intensity is drastically amplified. This phenomenon reveals that the failure risk of batteries under high-rate overcharging has shifted from the original heat accumulation to explosive venting, imposing higher requirements on the transient pressure relief and fire extinguishing design of energy storage systems.

(4) The guiding role of gas generation characteristics for fire safety in extreme environments has been evaluated. The variation laws of partial smoke toxic components with rate have been quantitatively uncovered, finding that the thermochemical decomposition of the electrolyte is most complete at the medium overcharge rate (2C), resulting in the highest gas toxicity index. This finding serves as a reminder that when formulating ventilation and decontamination strategies for confined spaces (such as underground parking lots or energy storage cabins), crucial attention must be paid to the chemical poisoning risks within specific rate intervals.

Acknowledgments

This work was supported by the National Key Research and Development Plan (2023YFC30099000), National Natural Science Foundation of China (52204221, 52104197, 52272396, 52474233), Hong Kong Scholar Program (XJ2022022), Opening Fund of State Key Laboratory of Fire Science (SKLFS) (HZ2024-KF10).

Declaration of competing interest

The authors declare that they have no known competing financial interests or personal relationships that could have appeared to influence the work reported in this paper.

References

1. Liu J, Huang D, Cui L, Zhang X, Wang Z, Tsai Y et al. Research progress on leakage and diffusion of CH4 and H2/CH4 in buried and submarine pipeline transportation processes. Emergency Management Science and Technology. 2025;5(1):e008. doi:10.48130/emst-0025-0007.

2. Moralı U. Importance of thermophysical properties of composite phase change materials in reducing lithium-ion battery temperature: a numerical and statistical approach. Journal of Thermal Analysis and Calorimetry. 2026. doi:10.1007/s10973-026-15697-9.

3. Selvakumar G, Senthilkumar T, Chandrasekar M, Arulmozhi S. Influences of notched fins configuration on thermo-electrical performance of flat solar photovoltaic cell. Journal of Thermal Analysis and Calorimetry. 2026. doi:10.1007/s10973-026-15782-z.

4. Ulusan E, Kılıç D, Kilikevičius A, Kale-Halasz G. Determinants of carbon emissions in Türkiye: globalization, energy consumption and passenger transportation. Journal of Thermal Analysis and Calorimetry. 2026. doi:10.1007/s10973-026-15371-0.

5. Wang W, Tao G, Zhang L. Comparative and analysis study of pool fire radiant heat models under different view factor calculations. Emergency Management Science and Technology. 2024;4(1):e003. doi:10.48130/emst-0024-0005.

6. Wang K, Li F, Zhang J, Yuan S, Wu X, Li M et al. Experimental and numerical study on the suppression mechanism of gas production and combustion in battery thermal runaway under overcharge conditions. Journal of Thermal Analysis and Calorimetry. 2025;150(19):15195-208. doi:10.1007/s10973-025-14644-4.

7. Ubelhor R, Ellison D, Hopkins CN, Hacker CD, Pirani B, Pol VG. Enhanced hazard characterization of lithium-ion batteries subject to destructive overcharge conditions. Journal of Thermal Analysis and Calorimetry. 2023;148(12):5403-21. doi:10.1007/s10973-023-12094-4.

8. Chen W, Ma B, Ma X, Zhang S, Jiang C, Bai G et al. Trigger-mode-dependent thermal runaway behavior and combustion characteristics of large-format lithium-ion cells for energy-storage applications. Journal of Thermal Analysis and Calorimetry. 2026. doi:10.1007/s10973-026-15465-9.

9. Gao P, Ji J, jia Z, Liu Y, Li J, Gao T et al. In-depth study on multiphase jet hazards of large-format cylindrical ternary batteries during thermal runaway. Journal of Energy Storage. 2026;142:119519. doi:https://doi.org/10.1016/j.est.2025.119519.

10. Chen W, Jiang J, Wen J. Thermal runaway induced by dynamic overcharge of lithium-ion batteries under different environmental conditions. Journal of Thermal Analysis and Calorimetry. 2021;146(2):855-63. doi:10.1007/s10973-020-10037-x.

11. Huang Y, Xu Y, Zhang P, Chen H, Huang R. In-depth study of gas-solid jet and formation mechanisms during thermal runaway in ternary lithium-ion batteries. Energy. 2025;324:135982. doi:https://doi.org/10.1016/j.energy.2025.135982.

12. Wang K, Wu D, Chang C, Zhang J, Ouyang D, Qian X. Charging rate effect on overcharge-induced thermal runaway characteristics and gas venting behaviors for commercial lithium iron phosphate batteries. Journal of Cleaner Production. 2024;434:139992. doi:https://doi.org/10.1016/j.jclepro.2023.139992.

13. Zhang Q, Guo B, Zhou G, Wang J, Song W, Huang Q et al. Preparation and mechanism

research of thermosensitive nanohydrogel for fire inhibition and reignition suppression in LFP battery. Fuel. 2026;407:137383. doi:https://doi.org/10.1016/j.fuel.2025.137383.
14. Wang Y, Wang Y, Xu C, Dai F, Zhang X, Wang H et al. Modeling study on fire propagation behavior and analysis of energy flow paths in double-layer LFP battery module. eTransportation. 2025;26:100508. doi:https://doi.org/10.1016/j.etran.2025.100508.
15. Liu Y-c, Li Y, Xue Z-a, Bai J-y. Three-dimensional thermo-electrochemical modeling of lithium dendrite penetration-induced separator failure and thermal runaway heat generation dynamics in lithium-ion batteries. Process Safety and Environmental Protection. 2025;204:108057. doi:https://doi.org/10.1016/j.psep.2025.108057.
16. Meng D, Wang Y, Wang J, Liu Z, Li H. Investigation of thermal runaway characteristics of lithium-ion battery under discharging condition coupled with thermal abuse. Process Safety and Environmental Protection. 2025;203:107877. doi:https://doi.org/10.1016/j.psep.2025.107877.
17. Zhou G, Liu Y, Yang S, Zhang Q, Li Y, Zhang X et al. Research on the thermal runaway mechanism and eruption flame dynamics of NCM811 lithium-ion battery stimulated by the coupling abuse of heat and penetration. Applied Thermal Engineering. 2024;253:123785. doi:https://doi.org/10.1016/j.applthermaleng.2024.123785.
18. Zhou H, Parmananda M, Crompton KR, Hladky MP, Dann MA, Ostanek JK et al. Effect of electrode crosstalk on heat release in lithium-ion batteries under thermal abuse scenarios. Energy Storage Materials. 2022;44:326-41. doi:https://doi.org/10.1016/j.ensm.2021.10.030.
19. Clerici D. POLISOC: A hybrid state of charge estimation algorithm for lithium-ion batteries based on electrical and mechanical measurements. Applied Energy. 2025;401:126740. doi:https://doi.org/10.1016/j.apenergy.2025.126740.
20. Liu S, Guo Q, Zhang J, Huang Z, Han D. Investigation on thermal runaway behaviors and gas generation dynamics of lithium-ion batteries induced by electrical abuse at low-pressure conditions. Journal of Energy Storage. 2025;125:116855. doi:https://doi.org/10.1016/j.est.2025.116855.
21. Oca L, Guillet N, Tessard R, Iraola U. Lithium-ion capacitor safety assessment under electrical abuse tests based on ultrasound characterization and cell opening. Journal of Energy Storage. 2019;23:29-36. doi:https://doi.org/10.1016/j.est.2019.02.033.
22. Li Z, Niu H, Jiang X. Simulation of electrical abuse of high-power lithium-ion batteries. Energy Procedia. 2017;142:3468-73. doi:https://doi.org/10.1016/j.egypro.2017.12.231.
23. Hu L, Yan J, Zhou M, Wei H. Temperature-dependent multi-physical modeling strategy and safety optimization of lithium-ion battery under mechanical abuses. Energy. 2025;329:136682. doi:https://doi.org/10.1016/j.energy.2025.136682.
24. Hu X, Li X, Shen Z, Wang Y, Yang J, Li J. Early safety warning method for lithium-ion batteries under mechanical abuse conditions based on online electrochemical parameter identification. Electrochimica Acta. 2025;542:147361. doi:https://doi.org/10.1016/j.electacta.2025.147361.
25. Guo Z, Ma Z, Liu J, Zhao W, Wang S, Zhao H et al. Overcharging cycle aging-induced severe degradation of safety properties of lithium-ion pouch battery cells subjected to mechanical abuse. Energy. 2025;320:135168. doi:https://doi.org/10.1016/j.energy.2025.135168.
26. Hahn A, Ruf M, Doose S, Kwade A. Enhancing lithium-ion battery safety: A comparative study of separator performance under mechanical abuse. Future Batteries. 2025;6:100064.

doi:https://doi.org/10.1016/j.fub.2025.100064.
27. Ren D, Feng X, Liu L, Hsu H, Ouyang M. Investigating the relationship between internal short circuit and thermal runaway of lithium-ion batteries under thermal abuse condition. Energy Storage Materials. 2021;34:563-73.
28. Wang G, Ping P, Kong D, Peng R, He X, Zhang Y et al. Advances and challenges in thermal runaway modeling of lithium-ion batteries. The Innovation. 2024;5(4):100624. doi:https://doi.org/10.1016/j.xinn.2024.100624.
29. Liu Y, Zhang L, Ding Y, Huang X, Huang X. Effect of thermal impact on the onset and propagation of thermal runaway over cylindrical Li-ion batteries. Renewable Energy. 2024;222:119910. doi:https://doi.org/10.1016/j.renene.2023.119910.
30. Feng X, Ren D, He X, Ouyang M. Mitigating Thermal Runaway of Lithium-Ion Batteries. Joule. 2020;4(4):743-70. doi:https://doi.org/10.1016/j.joule.2020.02.010.
31. Kvasha A, Gutiérrez C, Osa U, de Meatza I, Blazquez JA, Macicior H et al. A comparative study of thermal runaway of commercial lithium ion cells. Energy. 2018;159:547-57. doi:https://doi.org/10.1016/j.energy.2018.06.173.
32. Wang J, Yue Y, Yu K, Han C, Yang J, Zhang L et al. Thermal runaway behaviors of lithium iron phosphate battery with various capacity and state of charge: characteristic comparison and safety assessment. Applied Thermal Engineering. 2026;284:129170. doi:https://doi.org/10.1016/j.applthermaleng.2025.129170.
33. Huang Y, Zhao Y, Zhu N, Xu W, Lv J, Wang Z et al. Investigation on flame characteristic of lithium iron phosphate battery fires under different fire source-wall spacing. Journal of Energy Storage. 2025;108:115155. doi:https://doi.org/10.1016/j.est.2024.115155.
34. Wang J, Yu K, Xiao P, Li L, Wang C, Wang Z et al. Killing two birds with one stone strategy inspired advanced batteries with superior thermal safety: A comprehensive evaluation. Chemical Engineering Journal. 2025;515:163272. doi:https://doi.org/10.1016/j.cej.2025.163272.
35. Lin Z, Tong Z, Cai H, Li C, Ding Y, Lv C et al. Prelithiation technology for high energy density lithium-ion batteries: Design, progress, advantages and challenges. Energy Storage Materials. 2025;83:104709. doi:https://doi.org/10.1016/j.ensm.2025.104709.
36. Arshad F, Azam MU, Manurkar N, Zhang F, Idrees BS, Ahmad A et al. Life cycle assessment of lithium-ion and secondary batteries: A comparative analysis on environmental impacts and graphite recycling. eTransportation. 2026;27:100514. doi:https://doi.org/10.1016/j.etran.2025.100514.
37. Chen T, Jin H, Zhang C, Wang H. Lithium-ion battery remaining useful life prediction for portable medical device safety: a VMD-RVM based approach. Applications in Energy and Combustion Science. 2026;25:100432. doi:https://doi.org/10.1016/j.jaecs.2025.100432.
38. Galushkin NE, Yazvinskaya NN, Galushkin DN. Causes and mechanism of thermal runaway in lithium-ion batteries, contradictions in the generally accepted mechanism. Journal of Energy Storage. 2024;86:111372. doi:https://doi.org/10.1016/j.est.2024.111372.
39. Zhang J, Long T, Sun X, He L, Yang J, Wang J et al. Mechanism investigation on microstructure degradation and thermal runaway propagation of batteries undergoing high-rate cycling process. Journal of Energy Chemistry. 2026;113:1013-29. doi:https://doi.org/10.1016/j.jechem.2025.09.074.
40. Huang Y, Wang T, Xu W, Zhao Y, Liao Y, Wang J et al. Study on thermal runaway

characteristics of lithium batteries under high-rate charge/discharge and development of a deep learning-based early warning model. Energy. 2025;334:137676. doi:https://doi.org/10.1016/j.energy.2025.137676.
41. Wang J, Li L, Yu K, Zhang J, Huang Y, Wang Z et al. Comprehensive investigation on the water mist inhibition efficacy towards battery thermal runaway and its smoke hazard via regulating the releasing settings. Process Safety and Environmental Protection. 2025;204:108001. doi:https://doi.org/10.1016/j.psep.2025.108001.
42. Wang J, Yang J, Bai W, Wang Z, Yu K, Lu Y et al. Thermal runaway and jet flame features of LIBs undergone high-rate charge/discharge: An investigation. Journal of Energy Chemistry. 2025;103:826-37. doi:https://doi.org/10.1016/j.jechem.2024.12.004.
43. Chen L, Zeng S, Li J, Li K, Ma R, Liu J et al. Safety assessment of overcharged batteries and a novel passive warning method based on relaxation expansion force. Journal of Energy Chemistry. 2025;105:595-607. doi:https://doi.org/10.1016/j.jechem.2025.02.016.
44. Mao N, Geng X, Liu Y, Huang X, Hao M. Degradation behavior and underlying mechanisms of electrochemical and thermal stability in Li(Ni0.5Mn0.3Co0.2)O2/graphite lithium-ion batteries under overcharge conditions. International Communications in Heat and Mass Transfer. 2026;170:110029. doi:https://doi.org/10.1016/j.icheatmasstransfer.2025.110029.
45. Hu J, Zhang X, Wang Y, Wang T, Bi F, Sun L et al. A mechanistic modeling method for limited overcharge abuse of lithium-ion batteries. Energy. 2025;334:137645. doi:https://doi.org/10.1016/j.energy.2025.137645.
46. Ouyang D, Shen Y, Liu X, Shi D, Wang K, Zhi M et al. Investigation on thermal runaway features of large-format energy storage cells under overcharge scenarios. Applied Thermal Engineering. 2025;279:128051. doi:https://doi.org/10.1016/j.applthermaleng.2025.128051.
47. Kong D, Wang G, Wen JX. Propensity of 21700 cylindrical cells to thermal runaway under slight overcharging cycling – A numerical study. Process Safety and Environmental Protection. 2024;190:635-45. doi:https://doi.org/10.1016/j.psep.2024.07.097.
48. Yan WH, Huang WX, Yang Y, Wei ZW, Zhen HS, Lin Y. Research on overcharge mitigations and thermal runaway risk of 18650 lithium-ion batteries. Journal of Energy Storage. 2025;120:116372. doi:https://doi.org/10.1016/j.est.2025.116372.
49. Huang Y, Fan Y, Sun L, Shen X, Zhao Y, Cao Y et al. Mechanism of heat transfer suppression and safety evaluation of high-performance aerogel insulation materials in the thermal runaway propagation of lithium-ion batteries. Energy. 2025;334:137684. doi:https://doi.org/10.1016/j.energy.2025.137684.
50. Zhang X, Hu L, Delichatsios MA, Zhang J. Experimental study and analysis on flame lengths induced by wall-attached fire impinging upon an inclined ceiling. Proceedings of the Combustion Institute. 2019;37(3):3879-87. doi:https://doi.org/10.1016/j.proci.2018.06.203.
51. Huang Y, Zhao Y, Bai W, Cao Y, Xu W, Shen X et al. Study on the influence of high rate charge and discharge on thermal runaway behavior of lithium-ion battery. Process Safety and Environmental Protection. 2024;191:1483-94. doi:https://doi.org/10.1016/j.psep.2024.09.054.
52. Peng Y, Ding M, Zhang K, Zhang H, Hu Y, Lin Y et al. Quantitative Analysis of the Coupled Mechanisms of Lithium Plating, SEI Growth, and Electrolyte Decomposition in Fast Charging Battery. ACS ENERGY LETTERS. 2024;9(12):6022-8.
53. Liu J, Wang Z, Bai J. Influences of multi factors on thermal runaway induced by

overcharging of lithium-ion battery. Journal of Energy Chemistry. 2022;70:531-41. doi:https://doi.org/10.1016/j.jechem.2022.03.011.
54. Yang J, Ye W, Li W, Yang Y, Niu J, Xie J et al. Probabilistic multi-hazard coupling assessment framework for thermal runaway of aviation lithium-ion batteries: Integrating fuzzy logic and Monte Carlo simulation. Journal of Energy Storage. 2026;141:119137. doi:https://doi.org/10.1016/j.est.2025.119137.

Supplementary Files

This is a list of supplementary files associated with this preprint. Click to download.

- Hightlights.docx